Available online at www.sciencedirect.com

ScienceDirect

Geochimica et Cosmochimica Acta 120 (2013) 496–513

Geochimica et Cosmochimica Acta

www.elsevier.com/locate/gca

REE and Hf distribution among mineral phases in the CV–CK clan: A way to explain present-day Hf isotopic variations in chondrites

Céline Martin [a,*], Vinciane Debaille [b], Pierre Lanari [c], Steven Goderis [a,e], Isabelle Vandendael [d], Frank Vanhaecke [e], Olivier Vidal [f], Philippe Claeys [a]

[a] *Earth System Science, Vrije Universiteit Brussel, Pleinlaan 2, 1050 Brussels, Belgium*
[b] *Laboratoire G-Time, Université Libre de Bruxelles, Avenue F.D. Roosevelt 50, CP 160/02, 1050 Brussels, Belgium*
[c] *Institute of Geology, University of Bern, Baltzestrasse 1+3, Bern CH-3012, Switzerland*
[d] *Research Group Electrochemical and Surface Engineering, Vrije Universiteit Brussel, Pleinlaan 2, 1050 Brussels, Belgium*
[e] *Department of Analytical Chemistry, Ghent University, Krijgslaan 281 – S12, 9000 Ghent, Belgium*
[f] *ISTerre-CNRS UMR 5275, Maison des Géosciences, 1381, rue de la Piscine, 38400 Saint-Martin d'Hères, France*

Received 20 September 2012; accepted in revised form 4 July 2013; available online 15 July 2013

Abstract

Chondrites are among the most primitive objects in the Solar System and constitute the main building blocks of telluric planets. Among the radiochronometers currently used for dating geological events, Sm–Nd and Lu–Hf are both composed of refractory, lithophile element. They are thought to behave similarly as the parent elements (Sm and Lu) are generally less incompatible than the daughter elements (Nd and Hf) during geological processes. As such, their respective average isotopic compositions for the solar system should be well defined by the average of chondrites, called Chondritic Uniform Reservoir (CHUR). However, while the Sm–Nd isotopic system shows an actual spread of less than 4% in the average chondritic record, the Lu–Hf system shows a larger variation range of 28% [Bouvier A., Vervoort J. D. and Patchett P. J. (2008) The Lu–Hf and Sm–Nd isotopic composition of CHUR: Constraints from unequilibrated chondrites and implications for the bulk composition of terrestrial planets. *Earth Planet. Sci. Lett.* **273**, 48–57]. To better understand the contrast between Sm–Nd and Lu–Hf systems, the REE and Hf distribution among mineral phases during metamorphism of Karoonda (CK) and Vigarano-type (CV) carbonaceous chondrites has been examined. Mineral modes were determined from elemental mapping on a set of five CK chondrites (from types 3–6) and one CV3 chondrite. Trace-element patterns are obtained for the first time in all the chondrite-forming minerals of a given class (CK chondrites) as well as one CV3 sample. This study reveals that REE are distributed among both phosphates and silicates. Only 30–50% of Sm and Nd are stored in phosphates (at least in chondrites types 3–5); as such, they are not mobilized during early stages of metamorphism. The remaining fraction of Sm and Nd is distributed among the same mineral phases; these elements are therefore not decoupled during metamorphism. Of the whole-rock total of Lu, the fraction held in phosphate decreases significantly as the degree of metamorphism increases (30% for types 3 and 4, less than 5% in type 6). In contrast to Lu, Hf is mainly hosted by silicates with little contribution from phosphates throughout the CK metamorphic sequence. A significant part of Sm and Nd are stored in phosphates in types 3–5, and these elements behave similarly during CK chondrite metamorphism. That explains the robustness of the Sm/Nd ratios in chondrites through metamorphism, and the slight discrepancies observed in the present-day isotopic Nd values in chondrites. On the contrary, Lu and Hf are borne by several different minerals and consequently they are redistributed during

* Corresponding author. Present address: Earth and Planetary Sciences Department, American Museum of Natural History, Central Park West at 79th Street, New York, NY 10024-5192, USA. Tel.: +1 (212) 769 5365; fax: +1 (212) 769 5339.
E-mail address: cmartin@amnh.org (C. Martin).

0016-7037/$ - see front matter
http://dx.doi.org/10.1016/j.gca.2013.07.006

metamorphism–induced recrystallization. The Lu/Hf ratios are therefore significantly disturbed during chondrites metamorphism, leading to the high discrepancies observed in present-day Hf isotopic values in chondrites.

1. INTRODUCTION

Chondrites are the most primitive and undifferentiated meteorites. It is generally assumed that the Earth and other solid planets in the inner solar system formed by chondrite accretion, after which they differentiated. As such, the average chondritic composition for lithophile and refractory elements, the Chondritic Uniform Reservoir (CHUR), serves as a chemical reference for geochemical studies of the Earth and other planets. It also constitutes a reference for several radioactive isotopic systems, in particular ^{147}Sm–^{143}Nd and ^{176}Lu–^{176}Hf. Since the initial Earth is proposed to be chemically similar to CHUR, the evolution of the silicate part of the Earth (Bulk Silicate Earth) should be close to that of the CHUR (Jacobsen and Wasserburg, 1979). Knowing the initial composition of the Earth makes it possible to model the evolution of the terrestrial reservoirs (e.g. Jacobsen and Wasserburg, 1979; Blichert-Toft and Albarède, 1997). Recently, it appeared that while Nd isotopic composition of chondrites is relatively homogeneous (εNd from −5.40 to +2.73), Hf isotopic composition varies more widely (εHf from −20.40 to +5.87; Fig. 1, Blichert-Toft and Albarède, 1997; Patchett et al., 2004; Bouvier et al., 2008). The ε notation is defined using Hf as an example as $\varepsilon_{Hf} = \frac{^{176}Hf/^{177}Hf^{sample} - ^{176}Hf/^{177}Hf^{CHUR}}{^{176}Hf/^{177}Hf^{CHUR}} \times 10000$. In order to reduce the spread observed for the Lu–Hf system, Bouvier et al. (2008) suggested that CHUR Hf values can be calculated from type 1, 2 and 3 chondrites, i.e. excluding thermally metamorphized chondrites. While this may be a valid approach to determine more tightly constrained Lu–Hf parameters for CHUR, it is important to document the reasons for greater dispersion in parent/daughter ratios of the Lu–Hf system compared to Sm–Nd.

While little data are available on rare earth element (REE) and Hf contents in some minerals in meteorites, no study has yet focused solely on the distribution of REE and Hf among mineral phases. The REE budget is usually assumed to be dominated by phosphates in ordinary chondrites (OC) and oldhamite in enstatite chondrites (EC), (Yongheng et al., 1993; Brearley and Jones, 1998; Gannoun et al., 2011). The rare studies focusing on phosphates in OC so far demonstrate concentrations up to tens of ppm for REE, and less than 1 ppm of Hf (Amelin and Rotenberg, 2004; Amelin, 2005). The only study carried out on sulfides in OC (Kong et al., 2000) concluded that the LREE content could be up to few ppm with decreasing values toward HREE (~0.1 ppm). *In situ* analyses on carbonaceous chondrites (CV and CR) showed low REE concentrations in olivine and low-Ca pyroxene (0.01–0.1 and 0.1–0.5 times CI chondrites, respectively), but significantly higher values in high-Ca pyroxene (1–10 times CI chondrites) (Mason and Martin, 1974; Jacquet et al., 2012). However, none of these studies have investigated the possible variations in REE and Hf contents during metamorphism, especially as some mineral phases may be replaced by new phases.

A complete suite of CK chondrites as well as one CV3 sample were selected to address this issue. Carbonaceous chondrites are among the most pristine material of the Solar System (Brearley, 1997) and CK are the only carbonaceous meteorites that have undergone metamorphism from types 3–6. Studying pristine material that underwent metamorphism is important, as higher metamorphic types (4 and higher) seem to have a larger range in Lu/Hf (up to 28%, Patchett et al., 2004), compared to lower metamorphic types (below type 4; variations of 7%; Bouvier et al., 2008). One CV3 chondrite was also selected, because the CK and CV chondrites are assumed to share a closely related origin and are informally referred to as the CV–CK clan, (Weisberg et al., 2006).

The present work addresses the evolution of mineral modes during thermal metamorphism as well as the content of REE and Hf in mineral phases in CV3 and CK types 3–6. Mass balances are calculated for each sample and the distribution of REE and Hf among chondritic mineral phases will be discussed.

2. METEORITE SAMPLES, PREPARATION AND ANALYTICAL TECHNIQUES

2.1. Sample preparation

Three CK chondrites were selected from the collections of Antarctic meteorites from the NASA and National Institute of Polar Research of Tokyo (NIPR) to avoid weathering effects as much as possible. The samples include CK5 meteorites Elephant Moraine 92002 (EET92002) and Asuka-881277 (A-881277), CK6 meteorite Yamato-82191 (Y-82191), and African desert meteorites NWA 5956 (CK3), NWA5772 (CV3) and NWA 5798 (CK4).

Each sample was cut with a diamond wire saw at the Université Libre de Bruxelles (Belgium). No water or other fluid was used during sawing to avoid possible dissolution of some mineral phases, aqueous contamination or oxidation. The chondrite pieces (<2.5 cm in size) were then mounted in epoxy resin and polished with ethanol, again to minimize oxidation.

2.2. Analytical techniques

Samples were imaged using a scanning electron microscope (Jeol JSM-6400, Vrije Universiteit Brussel and Jeol JXA-8600, Université Libre de Bruxelles) to select representative areas of the bulk sample. Subsequently, compositional X-ray maps were acquired on the selected areas using an electron probe micro-analyzer (EPMA) Cameca SX100 or Cameca SXFive (Camparis, Université Pierre et Marie Curie, Paris 6, France) in wavelength-dispersive mode (WDS). The mapping conditions utilized 15 keV

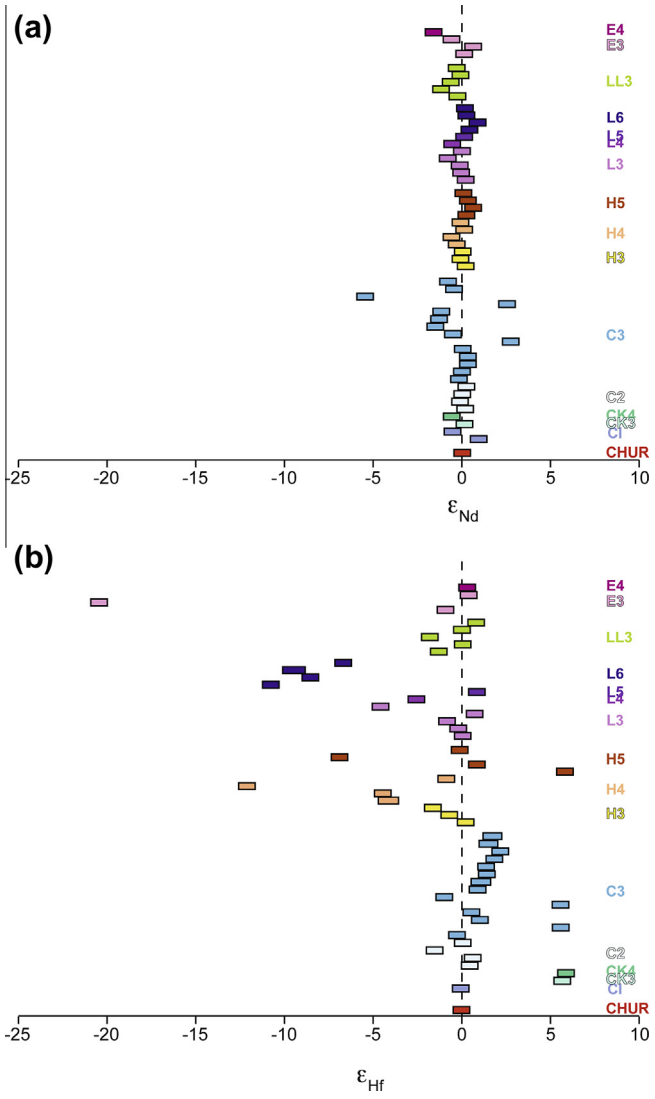

Fig. 1. Epsilon values in chondrites compared to CHUR. (a) for Nd and (b) for Hf. Only values from Patchett et al. (2004) and Bouvier et al. (2008) are presented here.

accelerating voltage, 100 nA beam current, and 100 ms counting time (De Andrade et al., 2006). These conditions enable maps to be measured up to 1500 × 1125 μm^2, with an analysis every 3 μm. Compositional X-ray maps were acquired for Si, Fe, Ca, Na, S, P, Ni, Cr and Mg. During the same microprobe session, spot analyses (standard conditions: 15 keV, 10 nA, 3 μm and 20 s) of all phases in the scanned area were also performed. These analyses are used as an internal standard to create element composition maps (oxide wt%) using the software XMapTools v1.5.1 (Lanari et al., 2012;Lanari, 2013; http://www.xmaptools.com).

For the determination of the trace element contents, whole rock aliquots were crushed in an agate mortar. Powdered samples (45–95 mg) were then digested in Teflon beakers in a mixture of HF and HNO_3 (2:1) and evaporated. After evaporation, HCl was added to ensure digestion of oxides and dissolution of fluoride that might have formed during the HF step. The resulting solutions were visually clear. Barium, REE, Hf, and Co concentrations were determined by ICP-MS (Element XR, Thermo Scientific) at Ghent University (Belgium). To monitor analytical reproducibility, geostandards BHVO-2 (USGS), and SRM694 (National Institute of Science and Technologies) were dissolved and analyzed under the same conditions. Reproducibility obtained on two duplicates was better than 5% for REE and 10% for Hf. Data are presented in Table 1.

In situ analyses of REE and Hf were performed using a New Wave Research UP193HE ArF* excimer-based laser ablation system coupled to an Element XR (ThermoScientific) double-focusing sector field ICP-MS instrument at Ghent University, Belgium. The following isotopes were monitored: ^{24}Mg, ^{29}Si, ^{44}Ca, ^{47}Ti, ^{57}Fe, ^{59}Co, ^{139}La, ^{140}Ce, ^{142}Ce, ^{141}Pr, ^{144}Nd, ^{146}Nd, ^{147}Sm, ^{152}Sm, ^{153}Eu ^{159}Tb, ^{163}Dy, ^{165}Ho, ^{166}Er, ^{169}Tm, ^{172}Yb, ^{174}Yb, ^{175}Lu, ^{178}Hf, ^{180}Hf. Analyses were performed using single spot

Table 1
Geostandards analyses and detection limits (all values in ppm).

Elements	BHVO-2G[a]	BHVO-2G (ICP-MS)	BHVO-2G (LA-ICP-MS)	NIST 694[b]	NIST 694 (ICP-MS)	BIR-1G[a]	BIR-1G (LA-ICP-MS)	GSD-1G[a]	GSD-1G (LA-ICP-MS)	Detection limits
Ba	131	132 ± 4	n.d.	111	102 ± 5		n.d.		n.d.	
Co	44	45 ± 1	34 ± 12		n.d.	52	55 ± 34	40	31 ± 3	7–30
La	15.2	15.5 ± 0.1	16.8 ± 0.6	98	92 ± 3	0.61	0.70 ± 0.20	39.1	40.5 ± 1.5	0.02–0.07
Ce	37.6	39.0 ± 0.6	28.1 ± 2.2	26	23 ± 0.2	1.89	2.30 ± 0.37	41.4	40.0 ± 1.5	0.01–0.06
Pr	5.35	5.49 ± 0.10	5.34 ± 0.20	n.d.	7 ± 0.2	0.37	0.39 ± 0.09	45	43.4 ± 1.6	0.01–0.04
Nd	24.5	25.5 ± 0.77	21.6 ± 1.1	48	45 ± 1	2.37	2.18 ± 0.49	44.7	39.7 ± 1.8	0.03–0.09
Sm	6.10	6.34 ± 0.19	5.84 ± 1.07	7.5	7 ± 0.2	1.09	1.12 ± 0.35	47.8	41.5 ± 2.9	0.02–0.05
Eu	2.07	2.06 ± 0.01	2.25 ± 0.38	1.7	1 ± 0.1	0.52	0.52 ± 0.19	41	40.4 ± 2.0	0.13–0.49
Gd	6.16	6.25 ± 0.13	5.95 ± 0.52	10.3	9 ± 0.2	1.85	1.79 ± 0.56	50.7	47.1 ± 2.6	0.28–0.71
Tb	0.92	0.98 ± 0.03	0.86 ± 0.08	1.4	1.3 ± 0.1	0.35	0.29 ± 0.10	47	42.8 ± 2.2	0.01–0.02
Dy	5.28	5.55 ± 0.14	5.53 ± 0.78	n.d.	8.5 ± 0.2	2.55	2.68 ± 0.65	51.2	48.9 ± 2.4	0.02–0.05
Ho	0.98	1.01 ± 0.03	1.00 ± 0.12	2.2	2.1 ± 0.1	0.56	0.49 ± 0.13	49	47.9 ± 2.6	0.01–0.03
Er	2.56	2.65 ± 0.07	2.46 ± 0.27	6.7	6.5 ± 0.2	1.70	1.46 ± 0.40	40.1	35.5 ± 2.8	0.01–0.09
Tm	0.34	0.36 ± 0.01	0.31 ± 0.10	1	1 ± 0.1	0.24	0.25 ± 0.08	49	45.7 ± 3.0	0.01–0.02
Yb	2.01	2.12 ± 0.06	2.09 ± 0.34	6	6 ± 0.1	1.64	1.56 ± 0.42	50.9	47.7 ± 3.4	0.01–0.02
Lu	0.28	0.29 ± 0.01	0.28 ± 0.06	1	1 ± 0.1	0.25	0.22 ± 0.09	51.5	48.6 ± 2.6	0.01–0.02
Hf	4.32	4.56 ± 0.12	4.41 ± 0.52	n.d.	0.4 ± 0.1	0.57	0.43 ± 0.19	39	37 ± 2	0.02–0.08

[a] Jochum and Stoll (2008).
[b] Hollocher et al. (1995).

(30 μm) ablation at a repetition rate of 10 Hz and a monitored energy density of ~10 J/cm^2 on the sample surface. Using ^{47}Ti as internal standard, quantification was performed via external calibration using several glass reference materials (USGS natural and synthetic glasses BHVO-2G, BIR-1G and GSD-1G). Based on the standards and settings described, external reproducibility for the elements measured was typically between 5% and 10% relative standard deviation (RSD; Table 1). The results obtained with Ti normalization were crosschecked with Ca or Mg normalization. The trace element concentrations presented in part 3.2 represent the averages on n measurements and the errors were calculated as the standard deviation divided by $\sqrt{n}$. Detection limits (Table 1) were calculated for each analysis as the trace element concentrations in the gas blank. The detection limits for Eu and Gd were significantly higher than for the other REE and mineral concentrations were only sporadically measured for these two elements. Although presented in *Trace element data* (Section 3.2.), the data for these two elements were not used further for mass balance calculations or to interpret trace elements patterns.

3. RESULTS

3.1. Petrology

Chemical variations within and between the phases present in the mapped areas were investigated using the modules Chem2D and TriPlot3D of XMapTools allowing all the compositions to be plotted in binary and ternary diagrams. The "Mask function" was used to create a 'mask image', i.e. to allocate all the pixels of the measured compositional map(s) to each of the occurring phases using a clustering approach (see Fig. 2b, d, f, h). From these mask images, modal abundances of each phase were calculated by the software. Two maps were acquired on CK5 EET92002 and CK6 Y-82191 to test the representativeness of the calculated modal abundance. Modal abundances of each sample are summarized in Table 2 and Fig. 3.

In sample NWA 5956 (CK3), back scattered electron (BSE) images reveal several chondrules of a maximum size of ~300 μm, sometimes rimmed by or including opaque minerals (Fig. 2a), as well as smaller chondrules (<100 μm) of opaque phases, embedded in the matrix. Fig. 2b presents the mask image obtained with XMapTools. The matrix, which is composed of a mixture of minerals with affinities to cronstedite, chrysotile and saponite, is the main component (63.8%). Glassy mesostasis (9.9%) is found as an interstitial phase inside the chondrules. Low-Ca pyroxene (15.4%) locally constitutes the main chondrule phase. The mapped area shows small (~250 μm) olivine (5.2%), always as euhedral crystals and almost always within chondrules. Taenite (<1%), generally weathered to lawrencite, is still present in the sample in close association with pyrrhotite (4.2%) and apatite (<1%).

NWA 5772 (CV3) has large chondrules (1–2 mm) with euhedral olivine crystals (17%) and low-Ca pyroxene (25.4%). Glassy mesostasis (8.7%) is found as an interstitial phase in the chondrules. The fine-grained matrix (47.3%) is rich in phyllosilicates. The only accessory phase present is magnetite (1.6%), either as relatively large crystals (up to 150 μm in length) inside the chondrules or as very small crystals (few microns) distributed within the matrix. Considering that this sample contains magnetite, not native Fe, and the matrix is composed of phyllosilicates, it belongs to the Bali-like oxidized subgroup (CV_{oxB}), in agreement with classifications of McSween (1977) and Weisberg et al. (1997).

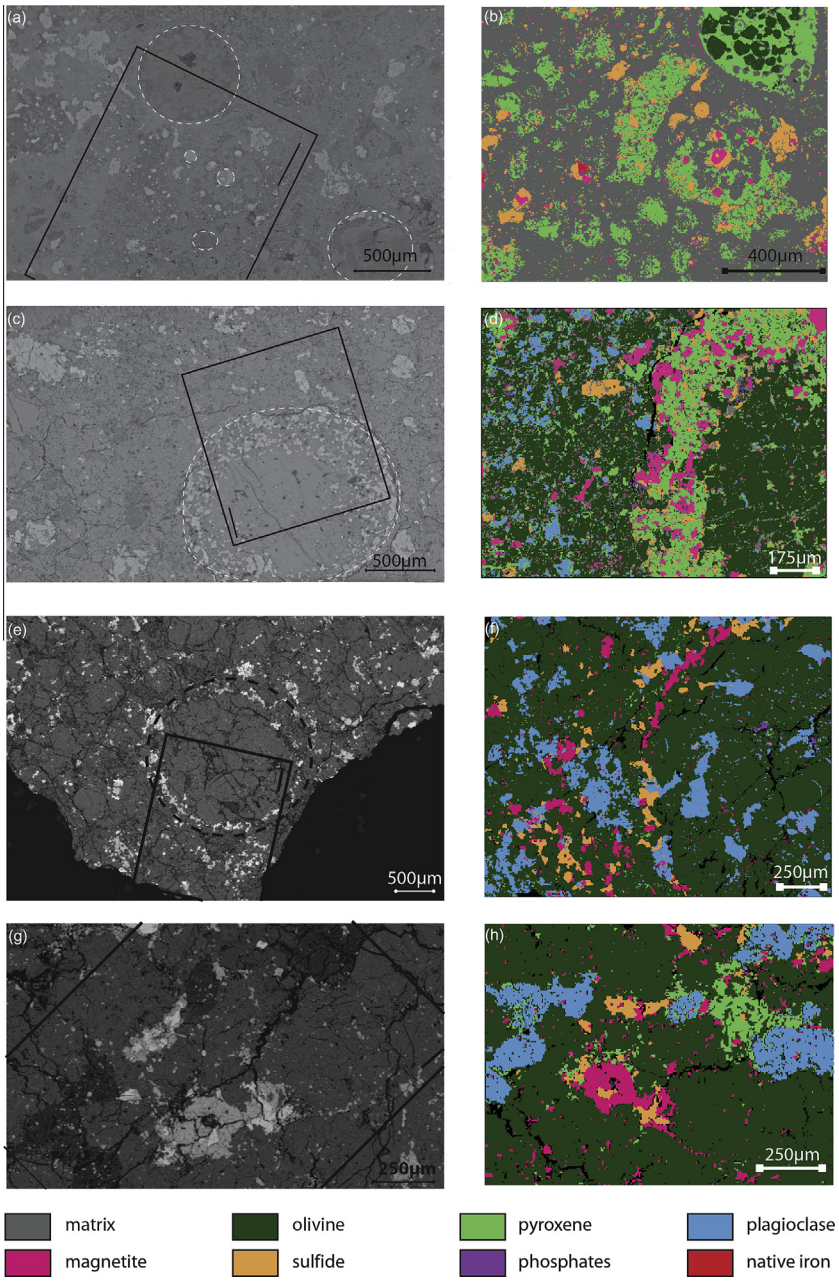

Fig. 2. (a) BSE and (b) mask image of CK3 NWA 5956, (c) BSE and (d) mask image of CK4 NWA 5798, (e) BSE and (f) mask image of CK5 EET92002, (g) BSE and (h) mask image of CK6 Y-82191. On BSE images, chondrules are highlighted with white dotted line and mask image area with black rectangle.

NWA 5798 (CK4) contains few chondrules (Fig. 2c) and those visible are overprinted by a rim of opaque phases and low-Ca pyroxene (14.6%), whereas the phyllosilicate-rich matrix is almost totally (9.4% remaining) recrystallized into olivine (54.1%) and plagioclase (4.2%). High-Ca pyroxene (5.3%) is xenomorphous. Clusters of pentlandite (3.6%) and magnetite (7.2%) with exsolutions of ilmenite, together with merrillite (<1%) are distributed throughout the matrix either found in association with opaque minerals or as single crystals (Fig. 2d).

In CK5 samples EET92002 and A-881277, only rare chondrules are discernible (Fig. 2e). Olivine crystals ($79.0 \pm 2.1\%$) are euhedral and large (up to 500 µm). Xenomorphous plagioclase ($8.0 \pm 5.5\%$) occurs both inside the chondrules and in the matrix, whereas xenomorphous low-Ca pyroxene (2.4%, only measurable in A-881277) and high-Ca pyroxene ($2.2 \pm 1.3\%$) are usually found in the matrix. The size ranges from ~30 µm for pyroxenes to ~100 µm for plagioclase. Pentlandite ($4.4 \pm 1.8\%$) and magnetite ($5.2 \pm 1.2\%$) are again found in close association,

Table 2
Modal abundances (%) obtained with XMapTools.

	NWA 5772	NWA 5956	NWA 5798	EET92 002(1)	EET92 002(2)	Average EET92002	A-881277	Average CK5	Y-82191(1)	Y-82191(2)	Average Y-191
Map size[a]	1500 × 1125	1200 × 900	1000 × 750	1500 × 1125	1200 × 900		1200 × 900		1000 × 750	1000 × 750	
Matrix	47.3	63.8	9.4	–	–		–		–	–	
Olivine	17.0	5.2	54.1	81.1	76.9	79.0 ± 3.0	79.0	79.0 ± 2.1	70.2	75.9	73.1 ± 4.0
Mesostasis	8.7	9.9	–	–	–		–		–	–	
Low-Ca pyroxene	25.4	15.4	14.6	–	–		2.4	2.4	–	–	
High-Ca pyroxene	–	–	5.3	3.1	0.7	1.9 ± 1.7	2.9	2.2 ± 1.3	7.0	5.2	6.1 ± 1.2
Plagioclase	–	–	4.2	5.9	14.2	10.0 ± 5.9	4.0	8.0 ± 5.5	11.0	7.1	9.0 ± 2.8
Phosphate	–	0.3	0.4	0.9	0.2	0.5 ± 0.5	0.8	0.6 ± 0.4	0.1	0.1	0.1 ± 0.0
Sulfide	–	4.2	3.6	2.9	3.8	3.4 ± 0.6	6.5	4.4 ± 1.8	3.2	2.1	2.6 ± 0.8
Magnetite	1.6	–	7.2	6.6	4.5	5.5 ± 1.5	4.5	5.2 ± 1.2	8.6	9.6	9.1 ± 0.8
Crack	–	–	1.1	–	–		–		–	–	
Total	100.0	100.0	99.9	100.5	100.3		100.0		100.0	100.0	

[a] Map sizes are given in μm.

locally surrounding chondrules (Fig. 2e). Merrillite crystals (0.6 ± 0.4%) display the largest sizes among all the CK chondrites studied (50–100 μm). They occur either in association with sulfide – magnetite or as single grains (Fig. 2f).

Chondrite Y-82191 (CK6) underwent the strongest metamorphism and the chondrules are not discernible (Fig. 2g). Olivine (73.1 ± 4%), plagioclase (9.1 ± 0.8%) and high-Ca pyroxene (6.1 ± 1.2%) are xenomorphous, whereas magnetite (9.1 ± 0.8%) is either xenomorphous or present as framboidal crystals. Xenomorphous sulfides (pentlandite and pyrrhotite, 2.6 ± 0.8%) as well as small merrillite (⩽10 μm, 0.1 ± 0%) are associated with magnetite (Fig. 2h). Rare and small crystals of spinel (⩽1 μm) occur in this sample.

3.2. Trace-elements data

The average trace element concentrations are normalized to the recent trace-element abundances for CI chondrites of Barrat et al. (2012). The REE and Hf patterns are reported for whole rock, magnetite, sulfides and silicates (two types of pyroxene, olivine, plagioclase and matrix) in all samples. In minerals, values are available only when the crystals are large enough to be measured (⩾30 μm). Due to the small size of the phosphate crystals, only two analyses were performed by LA-ICP-MS.

The whole-rock analyses show that all the CK samples are 1.5–2.5 times enriched in REE and Hf compared to CI chondrites (Fig. 4), except for Tm, Yb and Lu in CK5 A-881277 for which the concentrations are almost 3 times higher than in CI chondrites. The REE and Hf concentration patterns are slightly less fractionated with increasing metamorphism. Indeed, CK3 and CK4 samples have $(La/Yb)_N$ of 1.4 and 1.6, respectively, whereas CK5 EET92002 has a $(La/Yb)_N$ of 1.2 and CK6 an almost flat pattern ($(La/Yb)_N = 1$). Sample A-881277 (CK5) displays a singular HREE enriched-pattern, with $(La/Yb)_N = 0.7$. Sample CV3 NWA 5772 is enriched 1.3–1.5 times compared to CI chondrites (Fig. 4) and displays an almost flat pattern with $(La/Yb)_N = 1.1$. The Ba concentrations are systematically higher in samples coming from hot deserts (NWA 5772, NWA 5956, and NWA 5798) than in samples coming from Antarctica (EET92002, A-881277, and Y-82191, Table 3). This is likely due to weathering that is more important in hot desert than in Antarctica.

Most REE concentrations are similar in olivine for all CK chondrites and in CV3, even if La and Ce are lower in CK3 (Table 3). Hafnium contents usually range from 200 to 300 ppb in types 4–6 but are significantly lower in CK3 (~40 ppb) and higher in CV3 (~850 ppb). Olivines have slightly fractionated REE patterns (Fig. 5a), and are generally enriched in HREE compared to LREE ($(La/Yb)_N = 0.4$–0.7). The exception to this is CK5 A-881277 which is enriched in LREE compared to HREE ($(La/Yb)_N = 2.2$). A slight negative Ce anomaly is detected in olivine of NWA 5956 (CK3) and EET92002 (CK5), whereas olivine in NWA 5798 (CK4), A-881277 (CK5) and Y-191 (CK6) patterns have positive Ce anomalies. Except for NWA 5956 (CK3) that is 10 and 2 times depleted in LREE and HREE compared to CI chondrites, respectively, the other samples have values close to those of CI chondrites, slightly lower in LREE and slightly enriched (up to 3 times for Lu) for HREE (Fig. 5a).

In pyroxene, the REE contents vary according to the type of pyroxene. Low-Ca pyroxene has REE contents similar to those of olivines. The Hf values are more variable, ranging from 130 to 530 ppb in CK chondrites and less than 50 ppb in the CV3 chondrite. High-Ca pyroxene from samples NWA 5798 (CK4), EET92002 (CK5), and Y-82191 (CK6) have higher REE and Hf contents, with values up to several ppm (Table 3). Low-Ca pyroxene patterns are fractionated, with an increasing HREE enrichment corresponding to an increase in metamorphic degree with $(La/Yb)_N$ varying from 1.1 (CV3) to 0.3 (CK5); (Fig. 5b). High-Ca pyroxene is also fractionated ($(La/Yb)_N$ ranges from 0.4 to 0.6). Samples CK5 EET92002 and CK6 Y-82191 are enriched in REE approximately 10 times

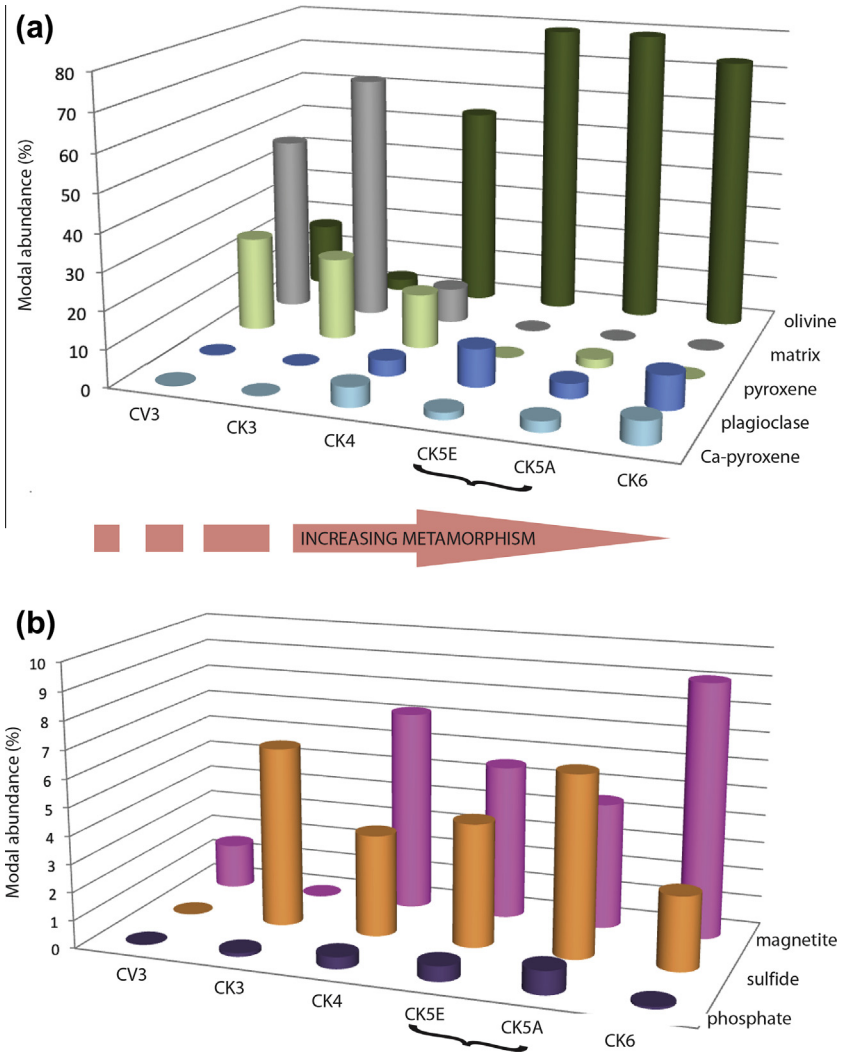

Fig. 3. Evolution of mineral abundances during thermal metamorphism. (a) Silicates and (b) accessory phases.

compared to low-Ca pyroxene, i.e. 4–5 times (LREE) to ~10 times (HREE) compared to CI chondrites. Sample CK4 NWA5798 is only 2–4 times higher in REE compared to CI chondrites, except Lu (0.9 times). The Hf values are about 10–15 times those of CI chondrites (Fig. 5b). High-Ca pyroxene patterns do not have any Ce anomalies, together with the low-Ca pyroxene in CK5 EET92002. On the contrary, low-Ca pyroxene patterns of CV3 NWA 5772 and CK4 NWA 5798 have significant positive Ce anomalies, and CK3 NWA 5956 has a slight negative Ce anomaly.

The matrix of type 3 chondrites is relatively enriched in REE compared to olivine and low-Ca pyroxene, with up several hundreds of ppb for LREE, a minimum of 30 ppb for HREE, and Hf contents are close to 200 ppb (Table 3). They have almost flat REE and Hf patterns ($(La/Yb)_N = 1$ (CV3) and 1.1 (CK3)) with a slight negative anomaly in Ce in CV3 NWA 5772 an a slight positive anomaly in Ce in CK3 NWA 5956. They are 2–3 times enriched in REE and Hf relative to CI chondrites (Fig. 5c).

REE concentrations in plagioclase appear quite variable, but the Hf concentrations are relatively homogeneous and range from 150 to 300 ppb (Table 3). It should be pointed out that the thin but elongated shape of the plagioclase renders analysis difficult considering the size of the laser beam (30 μm). In addition, concentrations in plagioclase are often below the detection limit of the LA-ICP-MS, explaining the data missing in Table 3. Plagioclases have fractionated patterns slightly enriched in LREE ($(La/Yb)_N > 2$ for CK4, and CK6), almost flat for CK5 EET92002 ($(La/Yb)_N = 1$) and even slightly enriched in HREE in CK5 A-881277 ($(La/Yb)_N = 0.8$). The enrichment is a factor 2 compared to CI chondrites. Only the CK5 EET92002 and CK6 samples are represented on Fig 4d due to the lack of values for CK4 and CK5 A-881277 (Table 3). They display a slight negative Ce anomaly.

Magnetite has variable elemental abundances and fractionation. Only Hf content shows systematic behavior and decreases notably from type 3 (~400 ppb) to type 6 chondrites (below detection limit; Table 3). Magnetites show

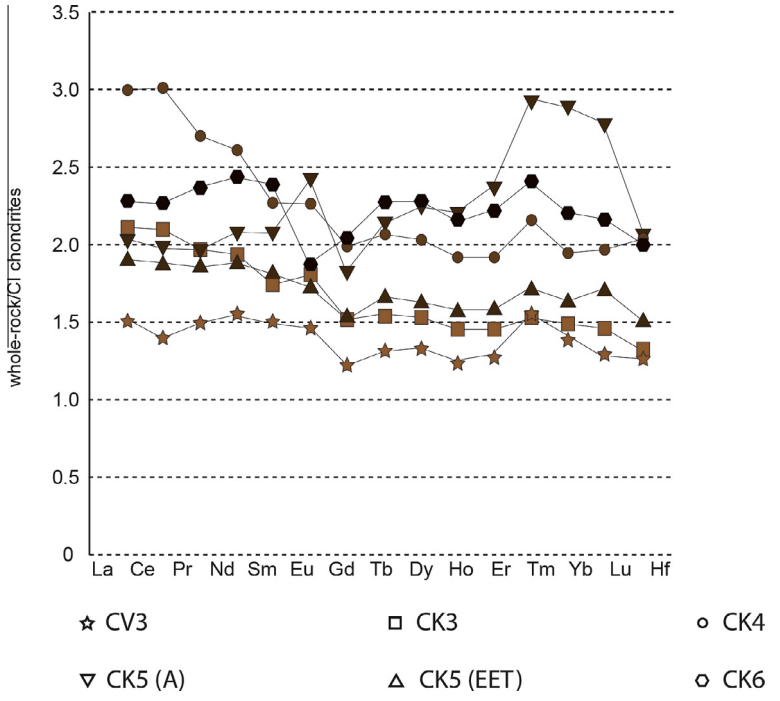

Fig. 4. Trace element patterns for whole-rocks normalized to CI chondrites (Barrat et al., 2012).

strongly varying patterns between the samples (Fig. 6a). Samples CV3 NWA5772 and CK5 A-881277 are very fractionated ($(La/Yb)_N$ ~6) but they have different trace element concentrations. NWA 5772 (CV3) is enriched compared to CI chondrite (22 to 3–4 times for LREE and HREE and Hf, respectively) whereas A-881277 (CK5) is depleted compared to CI chondrite (0.5–0.1 times for LREE and HREE respectively, 0.7 times for Hf). CK4 NWA 5798 and CK6 Y-82191 are less fractionated ($(La/Yb)_N$ of ~1.2) and they have similar contents, close to that of CI chondrites (1.2–2 times CI). CK5 EET92002 shows the opposite fractionation, in favor of HREE ($(La/Yb)_N$ = 0.6) and is depleted (0.3–0.75 times CI for LREE and HREE and Hf respectively). CK4 NWA 5798 and CK6 Y-82191 have slight positive Ce anomalies.

Sulfides have the lowest incompatible trace element contents among the accessory minerals analyzed. REE values often fall below detection limits. Hafnium ranges from 10 to 80 ppb (Table 3). Sulfides have slightly HREE enriched patterns ($(La/Yb)_N$ = 0.6–0.8). They are slightly depleted compared to CI chondrites (0.5–1 time). Hafnium ranges between 0.1 and 0.7 times CI values for all sample types (Fig. 6b).

Only one laser shot was possible on the small phosphate phases in NWA 5798 (CK4) and one in EET92002 (CK5). The results indicate that the two phosphates display different fractionation and contents. In CK4 NWA 5978, the pattern is almost flat ($(La/Yb)_N$ = 1.2) whereas it is fractionated in EET92002 ($(La/Yb)_N$ = 3.4) but both have a slight negative anomaly in Ce (Fig. 6c). Phosphate in NWA 5978 (CK4) appears more enriched (130–170 times CI chondrites) than phosphate in EET92002 (60–16 times CI chondrites for LREE and HREE, respectively; Fig. 5c). Hafnium is equal or slightly enriched compared to CI chondrite (1–2 times). Because only two points were analyzed, these results should be interpreted carefully.

3.3. Mass balance calculations

The fraction of a given element i borne by a given mineral min is: $F_i = \frac{[i]^{min} \times ab^{min} \times d^{min}}{[i]^{WR} \times \sum (ab^{min} \times d^{min})}$ where F_i (in %) is the fraction of i borne by the given mineral, $[i]^{min}$ and $[i]^{WR}$ the concentration of i in the mineral min (obtained by LA-ICPMS) and in the whole rock (obtained by ICPMS), respectively, ab^{min} the modal abundance of the given mineral (determined by XMapTools), and d^{min} the density of a given mineral. The densities used in the calculations are 3.3 for olivine, 3.4 for pyroxenes, 3.2 for phosphate, 4.8 for sulfide, 2.7 for plagioclase, 2.5 for the matrix and 5.1 for magnetite (Anthony et al., 2001).

The mass balances MB are:

$$MB = \sum F_i$$

Thus, the mass balances of REE and Hf should be equal to 100% (Table 4). The analytical errors on WR are up to 5% on REE and up to 10% for Hf. MB are therefore considered as satisfactory when they are comprised, within error, between 95% and 105% for REE and 90% and 110% for Hf.

In CV3 samples (Table 4), the phyllosilicate-rich matrix bears more than 30% of the LREE and MREE and up to 100% of the HREE. The remaining part is mostly in magnetite, with lesser amount in low-Ca pyroxene and olivine. In CK3, the REE are distributed almost equally among the phyllosilicate-rich matrix and phosphate and the remaining part is in low-Ca pyroxene.

Table 3
Trace element concentrations in whole-rocks and minerals (Co and Ba values are in ppm, REE and Hf values are in ppb, except in phosphates in which all elements are in ppm).

	CV3 NWA 5772	CK3 NWA 5956	CK4 NWA 5798	CK5 EET92002	CK5 A-881277	CK6 Y-82191
Whole-rock						
Ba	87.50 ± 0.05	30.65 ± 0.05	50.15 ± 0.30	6.10 ± 0.30	6.45 ± 0.10	4.20 ± 0.15
Co	464 ± 4	550 ± 3	580 ± 4	651 ± 10	684 ± 16	771 ± 0.5
La	360 ± 10	500 ± 10	710 ± 20	450 ± 10	480 ± 10	530 ± 10
Ce	860 ± 10	1280 ± 20	1830 ± 30	1140 ± 10	1210 ± 10	1380 ± 10
Pr	140 ± 10	190 ± 10	260 ± 10	180 ± 10	190 ± 10	220 ± 10
Nd	730 ± 30	900 ± 50	1220 ± 40	880 ± 30	960 ± 10	1130 ± 10
Sm	230 ± 10	270 ± 20	350 ± 30	270 ± 10	320 ± 10	360 ± 10
Eu	80 ± 10	110 ± 10	130 ± 10	100 ± 10	140 ± 10	110 ± 10
Gd	250 ± 10	310 ± 10	400 ± 10	310 ± 10	370 ± 10	410 ± 10
Tb	50 ± 10	60 ± 10	80 ± 10	60 ± 10	80 ± 10	80 ± 10
Dy	340 ± 10	390 ± 10	510 ± 10	410 ± 20	570 ± 10	570 ± 10
Ho	70 ± 10	80 ± 10	110 ± 10	90 ± 10	120 ± 10	120 ± 10
Er	210 ± 10	240 ± 10	320 ± 20	260 ± 10	390 ± 10	360 ± 10
Tm	40 ± 10	40 ± 10	50 ± 10	40 ± 10	70 ± 10	60 ± 10
Yb	240 ± 10	250 ± 10	330 ± 10	270 ± 10	490 ± 10	370 ± 10
Lu	30 ± 10	40 ± 10	50 ± 10	40 ± 10	70 ± 10	50 ± 10
Hf	140 ± 10	140 ± 10	220 ± 20	160 ± 20	220 ± 20	210 ± 20
Olivine						
Co	80 ± 28	33 ± 12	470 ± 75	n.d.	308 ± 106	461 ± 53
La	190 ± 50	50 ± 5	120 ± 20	260 ± 90	191 ± 35	140 ± 20
Ce	48 ± 160	60 ± 20	1250 ± 280	480 ± 160	1360 ± 830	960 ± 250
Pr	25 ± 5	20 ± 5	80 ± 5	100 ± 25	40 ± 10	120 ± 30
Nd	170 ± 70	140 ± 80	190 ± 40	600 ± 170	160 ± 60	165 ± 40
Sm	60 $n = 1$	40 ± 10	<d.l.	260 ± 70	50 ± 5	85 ± 10
Eu	<d.l.	<d.l.	210 $n = 1$	<d.l.	<d.l.	300 $n = 1$
Gd	<d.l.	<d.l.	330 $n = 1$	520 $n = 1$	<d.l.	420 ± 25
Tb	40 ± 5	15 ± 5	30 ± 10	50 ± 10	20 $n = 1$	50 ± 10
Dy	125 ± 30	100 ± 40	70 ± 10	270 ± 90	80 ± 10	90 ± 15
Ho	30 ± 5	15 ± 5	<d.l.	60 ± 20	25 ± 5	50 ± 5
Er	90 ± 20	40 ± 15	120 $n = 1$	330 ± 70	35 ± 10	130 ± 30
Tm	30 ± 10	5 ± 5	20 ± 5	50 ± 10	10 ± 5	30 ± 10
Yb	200 ± 40	80 ± 30	115 ± 30	440 ± 80	60 ± 15	140 ± 25
Lu	20 ± 5	15 ± 5	50 ± 10	80 ± 15	<d.l.	35 ± 5
Hf	840 ± 550	40 ± 10	200 ± 50	200 ± 40	90 ± 20	290 ± 30
n	7	6	13	7	7	9

Pyroxene							
	CV3 NWA 5772	CK3 NWA 5956	CK4 NWA 5798		CK5EET92002		CK6 Y-82191
	Low-Ca	Low-Ca	Low-Ca	High-Ca	Low-Ca	High-Ca	High-Ca
Co	64 ± 17	32 ± 5	320 ± 83	0.401	n.d.	n.d.	438 ± 182
La	110 ± 30	160 ± 40	130 ± 30	1530	100	1070	390 ± 90
Ce	805 ± 470	325 ± 100	4500 ± 1670	350	280	2840	4025 ± 670
Pr	25 ± 5	85 ± 20	50 ± 20	620	30	375	530 ± 60
Nd	80 ± 15	250 ± 50	225 ± 50	280	340	3090	2320 ± 270
Sm	35 ± 5	150 ± 20	120 ± 10	1175	60	1030	1270 ± 220
Eu	110 $n = 1$	<d.l.	300 ± 100	150	<d.l.	265	410 ± 45
Gd	<d.l.	440 $n = 1$	<d.l.	900	<d.l.	1320	1540 ± 200
Tb	30 ± 10	30 ± 10	45 ± 5	140	<d.l.	260	340 ± 40
Dy	60 ± 10	130 ± 30	200 ± 30	530	170	1895	2490 ± 430
Ho	40 $n = 1$	40 ± 10	40 ± 15	70	<d.l.	390	565 ± 80
Er	50 ± 10	130 ± 30	110 ± 20	750	170	1690	1920 ± 160
Tm	20 ± 5	20 ± 5	45 ± 20	20	30	230	280 ± 40
Yb	70 ± 10	160 ± 30	300 ± 60	1000	225	1340	1510 ± 240
Lu	10 ± 5	25 ± 5	90 ± 40	400	65	275	220 30
Hf	45 ± 15	130 ± 30	530 ± 260	1530	180	1670	1015 ± 270
n	5	10	7	1	1	1	5

	Matrix		Plagioclase			
	CV3 NWA 5772	CK3 NWA 5956	CK4 NWA 5798	CK5 EET92002	CK5 A-881277	CK6 Y-82191
Co	319 ± 42	365 ± 146	93 ± 53	n.d.	98 ± 37	197 ± 57
La	650 ± 60	310 ± 50	330 ± 50	380 ± 85	470 ± 60	1825 ± 385
Ce	860 ± 90	1150 ± 370	12470 ± 7690	440 ± 100	15200 ± 12030	2420 ± 875
Pr	170 ± 30	90 ± 15	<d.l.	90 ± 20	120 ± 60	630 ± 340
Nd	550 ± 110	310 ± 40	<d.l.	540 ± 180	<d.l.	1410 ± 790
Sm	430 ± 40	160 ± 30	240 ± 70	190 ± 40	80 ± 40	540 ± 150
Eu	<d.l.	<d.l.	280 $n = 1$	350 ± 100	670 $n = 1$	1550 ± 85
Gd	700 ± 60	600 ± 75	<d.l.	<d.l.	<d.l.	2590 $n = 1$
Tb	90 ± 15	40 ± 5	<d.l.	30 ± 10	30 $n = 1$	100 $n = 1$
Dy	300 ± 60	180 ± 40	420 $n = 1$	150 ± 70	440 $n = 1$	1265 ± 10
Ho	90 ± 25	50 ± 10	195 $n = 1$	55 ± 20	40 ± 5	260 $n = 1$
Er	290 ± 60	180 ± 30	<d.l.	150 ± 60	<d.l.	510 $n = 1$
Tm	40 ± 5	30 ± 5	110 $n = 1$	50 ± 15	40 ± 5	<d.l.
Yb	390 ± 60	200 ± 35	100 $n = 1$	275 ± 70	440 $n = 1$	560 $n = 1$
Lu	85 ± 20	40 ± 10	160 ± 80	60 $n = 1$	<d.l.	75 $n = 1$
Hf	170 ± 20	210 ± 60	300 ± 140	150 ± 80	290 ± 140	240 ± 100
n	9	12	2	6	2	3

Magnetite

	CV3 NWA 5772	CK4 NWA 5798	CK5 EET92002	CK5 A-881277	CK6 Y-82191
Co	2420 ± 1220	91 ± 40	n.d.	12 ± 4	524 $n = 1$
La	5210 ± 1340	490 ± 110	70 ± 15	115 <d.l.	370 ± 85
Ce	13820 ± 6030	1790 ± 940	240 ± 115	160 ± 140	4770 ± 4010
Pr	950 ± 200	45 ± 15	25 ± 5	15 ± 10	150 ± 30
Nd	5070 ± 1280	580 ± 195	160 ± 30	130 ± 60	515 ± 410
Sm	1355 ± 590	610 ± 270	70 ± 25	10 ± 10	600 ± 250
Eu	810 ± 145	270 ± 35	<d.l	<d.l	<d.l
Gd	1680 ± 250	625 $n = 1$	<d.l	<d.l	<d.l
Tb	300 ± 85	30 ± 20	30 $n = 1$	5 ± 5	50 5
Dy	1290 ± 400	340 $n = 1$	80 ± 50	<d.l	250 ± 30
Ho	260 ± 130	60 ± 30	30 ± 5	5 $n = 1$	<d.l.
Er	870 ± 130	230 ± 100	100 ± 20	<d.l	140 ± 40
Tm	150 ± 60	<d.l	30 ± 5	5 $n = 1$	40 ± 20
Yb	640 ± 180	290 ± 110	90 ± 30	15 $n = 1$	210 $n = 1$
Lu	135 ± 25	<d.l	20 ± 5	<d.l	70 $n = 1$
Hf	390 ± 80	310 ± 125	75 ± 50	75 ± 30	<d.l
n	6	4	5	2	2

	Sulphide					Phosphate	
	CK3 NWA 5956	CK4 NWA 5798	CK5 EET-92002	CK5 A-881277	CK6 Y-82191	CK4 NWA 5798	CK5 EET-92002
Co	1040 ± 410	235 ± 80	n.d.	12420	200	45	n.d.
La	50 ± 10	5 ± 5	230 ± 50	110	110	40	15
Ce	215 ± 60	15 ± 5	550 ± 100	280	510	81	26
Pr	30 ± 10	< d.l.	70 ± 15	15	110	14	5
Nd	<d.l.	5 ± 5	460 ± 100	280	35	69	30
Sm	<d.l.	<d.l.	170 ± 10	<d.l.	<d.l.	26	9
Eu	<d.l.	5 $n = 1$	<d.l.	<d.l.	<d.l.	9	2
Gd	<d.l.	<d.l.	410 $n = 1$	<d.l.	<d.l.	33	7
Tb	50 $n = 1$	5 $n = 1$	30 ± 10	<d.l.	50	6	1
Dy	85 $n = 1$	5 $n = 1$	210 ± 30	40	<d.l.	47	6.5
Ho	15 ± 5	5 $n = 1$	50 ± 10	20	75	10	1
Er	30 ± 5	5 $n = 1$	210 ± 30	80	<d.l.	28	4
Tm	<d.l.	5 $n = 1$	40 ± 10	40	15	4	0.5
Yb	<d.l.	5 $n = 1$	270 ± 40	100	110	24	3
Lu	<d.l.	<d.l.	50 ± 5	<d.l.	50	3	0.4
Hf	80 ± 10	10 ± 5	65 ± 10	80	30	0.24	0.10
n	6	3	5	1	1	1	1

n.d.: not determined. <d.l.: below detection limit. n = number of analyses.

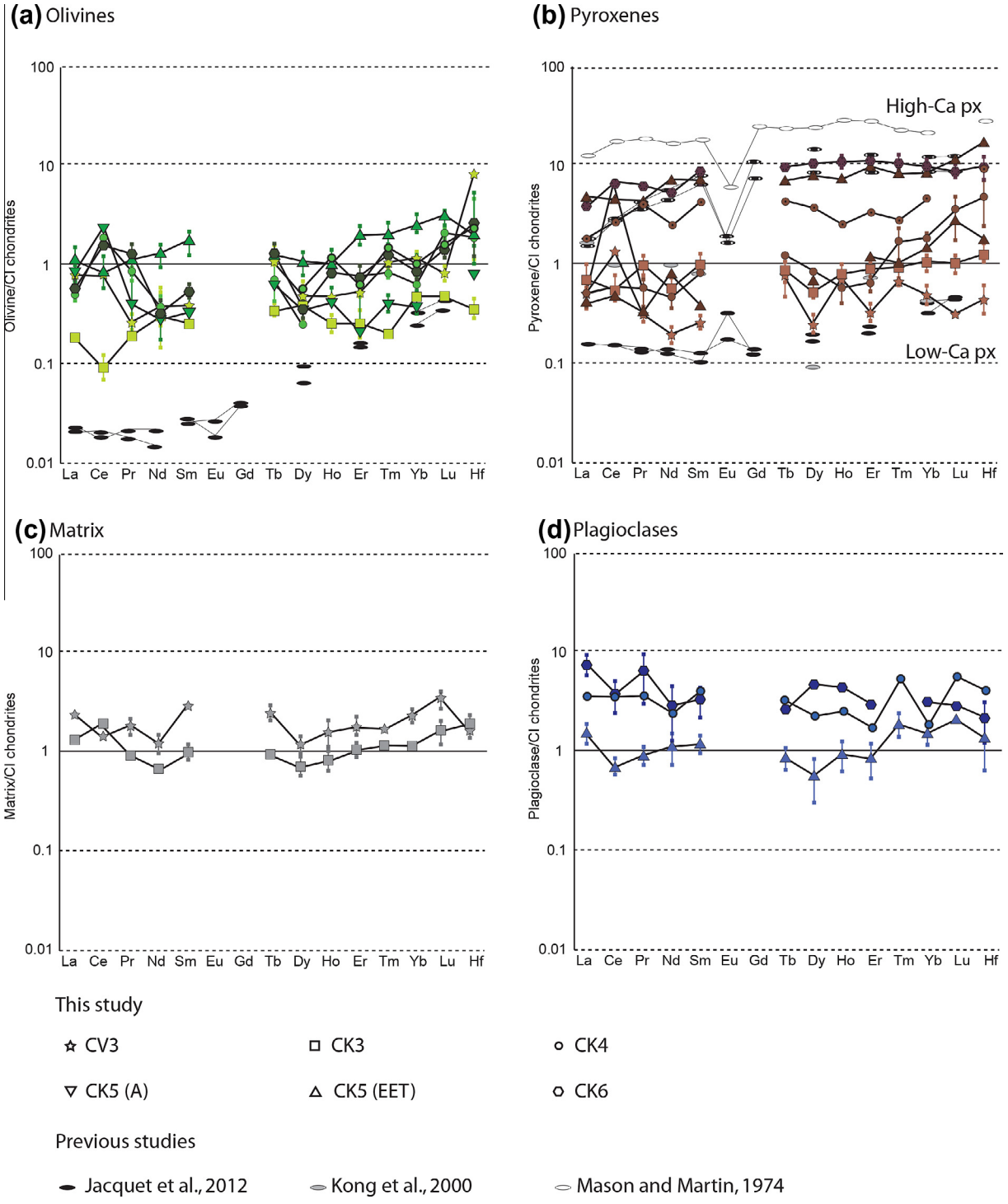

Fig. 5. Trace element patterns for silicates normalized to CI chondrites (Barrat et al., 2012) and comparison with other published data. (a) Olivine, (b) pyroxene, (c) matrix and (d) plagioclase.

Hafnium is mainly distributed among silicates in type 3 CK and CV chondrites. In CV3, the major part is found in olivine and the remaining fraction occurs in the matrix and low-Ca pyroxene. In CK3, Hf is mostly in the matrix with lesser amount in low-Ca pyroxene. Totals are rather satisfying for both CV3 and CK3, even if they are slightly too low for LREE and satisfying, even too high for HREE and Hf. This might be due to the lack of REE measurements in mesostasis.

In CK4 NWA 5798 (Table 4), REE are mainly distributed among phosphate and olivine. The remaining part is found in high-Ca pyroxene, low-Ca pyroxene, plagioclase, residual matrix and magnetite. Hafnium is mainly distributed among olivine, high-Ca pyroxene and low-Ca

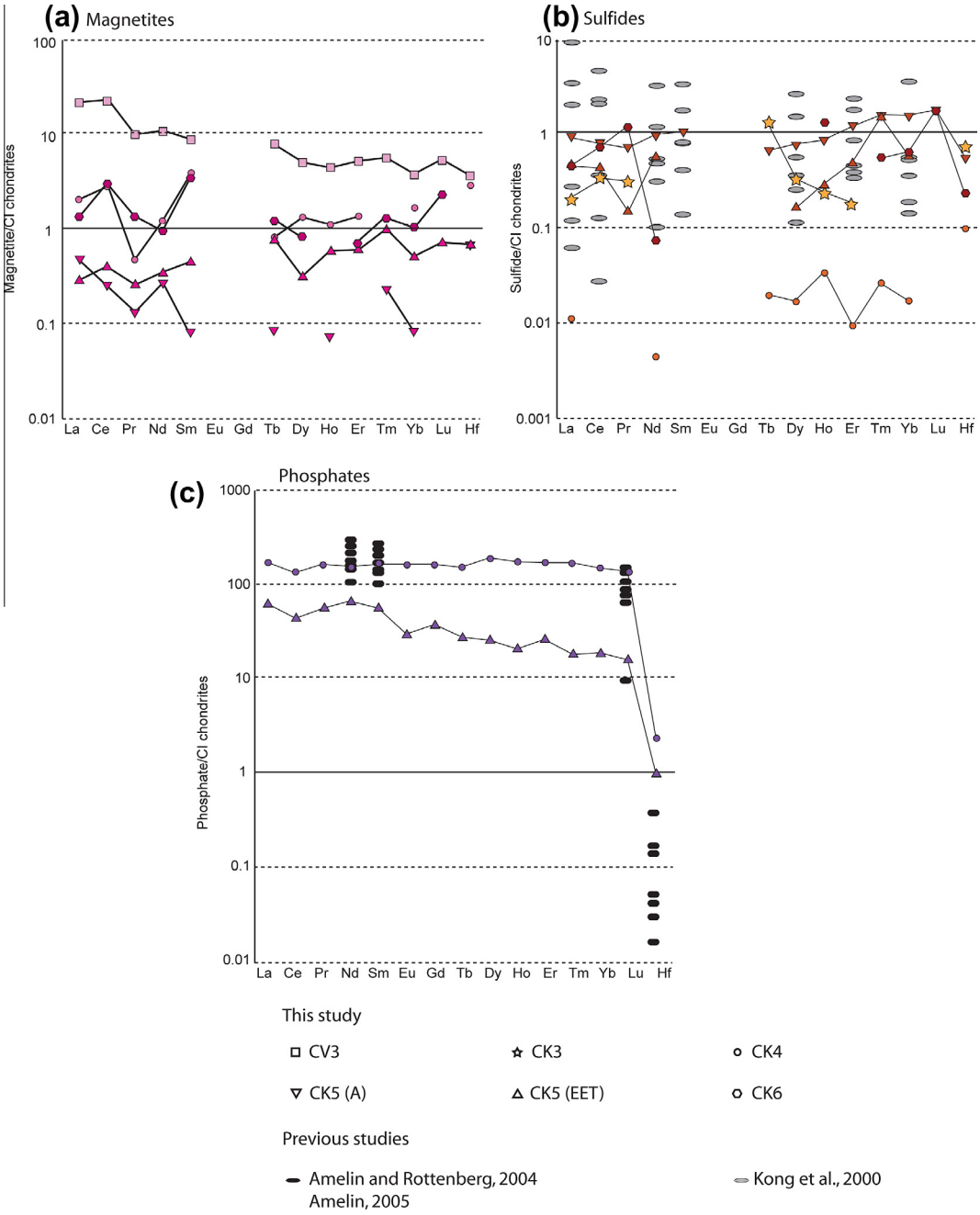

Fig. 6. Trace element patterns for accessory phases normalized to CI chondrites (Barrat et al., 2012) and comparison with other published data. (a) Magnetite, (b) sulfide, and (c) phosphate.

pyroxene. Lower amounts are distributed among magnetite, matrix and plagioclase. The part of Ce borne by silicates is significantly higher than for the other LREE, likely due to the two oxidation states of this element. Nevertheless, the recalculated total of Ce is reasonably satisfactory ($138 \pm 24\%$). For the other elements, the mass balances are too low, except for HREE. Lutetium and Hf are even slightly too high.

The CK5 samples highlight significant differences in their trace-element distribution (Table 4). In EET92002, the main carriers of REE are olivine and phosphate. High-Ca pyroxene, sulfide and magnetite display an increasing contribution in the mass-balance toward the HREE, but remain below 12%. Hafnium is distributed among olivine, high-Ca pyroxene, plagioclase, magnetite and sulfide. The totals are satisfying for most of the REE, except for Ce and Pr, (too low) and the HREE and Hf, (too high). A-881277 shows that the REE are distributed mainly among phosphate, while the remaining part is found in olivine, plagioclase and high-Ca pyroxene. Hafnium is

Table 4
Mass balance calculations (values in %).

	La	Ce	Pr	Nd	Sm	Eu	Gd	Tb	Dy	Ho	Er	Tm	Yb	Lu	Hf
CV3															
Olivine	10.0	10.4	3.3	4.5	4.9	/	/	15.3	6.9	7.1	7.8	12.8	16.1	11.8	115.5
±	*2.4*	*3.2*	*0.4*	*1.7*	*0.1*	/	/	*0.4*	*1.5*	*1.0*	*1.3*	*2.5*	*3.1*	*1.3*	*68.6*
Low-Ca px	8.8	27.0	5.2	3.1	4.4	37.4	/	15.3	4.9	15.5	6.6	11.4	8.9	6.0	9.4
±	*2.3*	*13.9*	*0.5*	*0.4*	*0.1*	/	/	*5.2*	*0.6*	/	*1.2*	*0.8*	*1.4*	*0.8*	*2.7*
Matrix	62.6	39.3	46.8	29.9	74.0	/	110.0	73.1	34.5	48.9	54.4	41.4	64.8	101.9	50.1
±	*7.1*	*5.1*	*9.2*	*6.8*	*7.9*	/	*11.2*	*13.2*	*7.7*	*16.9*	*13.4*	*6.1*	*12.2*	*23.3*	*5.1*
Magnetite	39.9	43.7	18.3	14.1	12.9	26	18.2	16.7	10.4	10.1	11.3	10.0	7.4	11.2	7.8
±	*6.00*	*11.2*	*2.3*	*2.8*	*4.0*	*2.6*	*1.5*	*2.7*	*1.9*	*2.9*	*0.9*	*2.3*	*1.2*	*1.1*	*0.9*
Total	**121.2**	**120.4**	**73.5**	**56.4**	**99.3**	**63.4**	**128.1**	**120.4**	**56.8**	**81.6**	**80.1**	**75.6**	**97.3**	**130.9**	**182.8**
±	***9.8***	***18.8***	***9.6***	***7.5***	***8.9***	***2.6***	***11.3***	***14.4***	***8.1***	***17.1***	***13.5***	***7.0***	***12.7***	***23.4***	***68.9***
CK3															
Olivine	0.6	0.3	0.6	0.9	0.9	/	/	1.4	1.6	1.1	1.1	0.8	2.0	2.0	1.6
±	*0.1*	*0.1*	*0.1*	*0.5*	*0.1*	/	/	*0.2*	*0.5*	*0.2*	*0.3*	/	*0.7*	*0.1*	*0.3*
Low-Ca px	5.9	4.7	8.5	5.1	10.2	/	26.4	9.3	6.2	8.6	9.8	9.7	11.7	11.6	17.1
±	*1.2*	*1.2*	*1.6*	*0.8*	*1.4*	/	/	*1.8*	*1.2*	*1.8*	*1.9*	*1.9*	*1.8*	*2.0*	*3.2*
Matrix	35.3	51.3	27.6	19.8	33.1	/	111.2	35.5	26.7	33.5	42.2	43.9	45.5	64.7	85.3
±	*5.9*	*18.3*	*4.7*	*2.6*	*6.2*	/	*15.3*	*4.5*	*6.1*	*8.4*	*7.7*	*6.3*	*8.7*	*19.6*	*26.2*
Sulfide	0.7	1.2	1.1	/	/	/	/	6.5	1.6	1.2	0.9	/	/	/	4.1
±	*0.1*	*0.2*	*0.1*	/	/	/	/	/	/	/	*0.1*	/	/	/	*0.4*
Phosphate[a]	25.0	19.9	24.6	24.4	30.2	28.2	34.1	30.5	38.1	37.7	37.5	35.2	30.7	27.8	0.5
Total	**67.5**	**77.3**	**62.3**	**50.2**	**74.2**	**28.2**	**171.7**	**83.1**	**74.2**	**82.1**	**91.5**	**89.6**	**89.8**	**106.1**	**108.6**
±	***6.0***	***18.3***	***5.0***	***2.7***	***6.3***	***1***	***15.3***	***4.8***	***6.2***	***8.6***	***8.0***	***6.6***	***8.9***	***19.7***	***26.4***
CK4															
Olivine	8.9	36.1	16.2	8.1	/	84.9	43.9	19.0	7.3	/	20.2	22.2	18.3	56.6	48.8
±	*1.4*	*8.2*	*0.6*	*1.6*	/	/	/	*4.2*	*1.0*	/	/	*4.4*	*4.4*	*7.4*	*10.7*
Low-Ca pyroxene	2.6	36.2	3.0	2.7	5.1	34.3	/	8.5	5.8	4.9	5.0	12.3	13.7	26.0	35.9
±	*0.7*	*13.3*	*1.0*	*0.6*	*0.5*	*10.2*	/	*0.2*	*0.7*	*1.6*	*0.7*	*4.3*	*2.6*	*12.1*	*16.9*
Plagioclase	1.6	23.0	/	/	2.3	7.2	/	/	2.8	6.1	/	6.9	1.0	11.0	4.7
±	*0.3*	*17.7*	/	/	*0.8*	/	/	/	/	/	/	/	/	*6.8*	*2.6*
Magnetite	7.6	10.7	1.9	5.2	19	22.7	16.9	4.4	7.2	6.4	7.9	/	9.7	/	15.6
±	*1.1*	*3.7*	*0.4*	*1.2*	*5.4*	*1.8*	/	*1.5*	/	*2.0*	*2.4*	/	*2.4*	/	*4.0*
Sulfide	<0.1	0.2	/	<0.1	/	0.1	/	<0.1	<0.1	<0.1	<0.1	<0.1	<0.1	/	0.2
±	/	/	/	/	/	/	/	/	/	/	/	/	/	/	*0.1*
High-Ca pyroxene	3.0	5.0	7.3	4.8	9.5	11.5	15.6	10.6	9.5	6.8	9.0	6.8	12.2	2.4	24.7
Phosphate	29.3	23.1	29.6	29.9	36.8	37.8	43.0	37.7	47.8	47.3	47.0	41.6	39.1	34.2	0.6
Matrix[b]	3.1	4.4	2.4	1.8	3.1	/	10.4	3.2	2.5	3.1	3.9	3.8	4.3	5.9	6.5
Total	**56.1**	**138.3**	**60.4**	**52.5**	**77.4**	**198.4**	**129.8**	**83.5**	**82.9**	**74.6**	**93.0**	**93.7**	**98.4**	**136.0**	**136.9**
±	***1.9***	***23.9***	***1.2***	***2.0***	***5.5***	***10.4***	***1***	***4.4***	***1.2***	***2.6***	***2.5***	***6.2***	***5.7***	***15.7***	***20.6***
CK5 EET92002															
Olivine	44.1	32.1	43.9	43.3	72.7	/	128.5	59.6	51.0	51.6	96.9	92.6	122.6	136.3	95.9
±	*16.7*	*11.3*	*10.9*	*15.3*	*21.0*	/	*2.7*	*15.7*	*17.0*	*15.9*	*21.9*	*21.9*	*23.9*	*26.4*	*15.4*
Plagioclase	6.7	3.1	4.0	4.6	9.9	28.4	/	4.3	2.9	5.0	4.5	9.3	8.0	10.4	7.6
±	*5.4*	*2.5*	*3.2*	*4.2*	*4.4*	*23.5*	/	*3.5*	*2.8*	*4.3*	*4.0*	*7.6*	*6.5*	*7.7*	*7.6*
High-Ca pyroxene	4.5	4.7	4.0	6.7	7.1	5.0	8.0	8.0	8.8	8.5	12.3	9.8	9.2	12.1	19.9
Magnetite	1.3	1.8	1.2	1.5	2.1	/	/	3.9	1.7	3.2	3.3	4.9	2.7	3.6	3.9
±	*0.3*	*0.6*	*0.3*	*0.3*	*0.6*	/	/	*0.7*	*0.7*	*0.6*	*0.7*	*1.0*	*0.8*	*0.9*	*1.9*
Sulfide	2.4	2.3	1.8	2.5	2.9	/	6.3	2.1	2.4	2.8	3.9	4.6	4.7	5.0	1.9
±	*0.5*	*0.4*	*0.4*	*0.5*	*0.4*	/	*0.8*	*0.5*	*0.4*	*0.5*	*0.7*	*0.8*	*0.8*	*0.8*	*0.2*
Phosphate	16.7	11.7	14.5	17.5	16.1	8.6	12.2	8.2	8.1	8.7	8.5	5.4	5.7	4.7	0.3
Total	**75.7**	**55.7**	**69.4**	**86.2**	**106.6**	**42.0**	**155.0**	**86.2**	**74.8**	**77.8**	**129.5**	**126.6**	**152.9**	**172.0**	**129.6**
±	***17.5***	***11.6***	***11.3***	***15.8***	***21.4***	***23.5***	***2.8***	***16.1***	***17.3***	***16.5***	***22.3***	***23.3***	***24.8***	***27.6***	***17.3***
CK5 A-881277															
Olivine	30.0	84.9	15.2	12.2	11.9	/	/	22.0	10.6	15.2	6.8	11.3	9.8	/	30.9
±	*5.8*	*54.4*	*4.4*	*4.9*	*0.8*	/	/	/	*1.2*	*2.4*	*1.4*	*2.4*	*2.4*	/	*6.3*
Plagioclase	3.0	39.1	2.0	/	0.8	15.0	/	1.1	2.4	1.0	/	1.6	2.8	/	4.1
±	*0.5*	*39.6*	*1.3*	/	*0.5*	/	/	/	/	*0.1*	/	*0.2*	/	/	*2.4*
Magnetite	1.6	0.9	0.4	0.9	0.3	/	/	0.3	/	0.2	/	0.5	0.2	/	2.2
±	/	*0.5*	*0.2*	*0.3*	*0.1*	/	/	*0.1*	/	/	/	/	/	/	*0.6*
Sulfide	2.1	2.1	0.7	2.6	0.0	/	/	/	0.7	1.3	1.9	4.8	1.8	/	3.2

Table 4 (*continued*)

	La	Ce	Pr	Nd	Sm	Eu	Gd	Tb	Dy	Ho	Er	Tm	Yb	Lu	Hf
Low-Ca pyroxene	0.5	0.5	0.5	0.8	0.4	/	/	/	0.7	/	1.0	0.8	1.1	2.2	1.9
High-Ca pyroxene[c]	6.3	6.6	5.7	9.0	9.2	5.3	9.9	9.3	9.4	8.9	12.2	8.6	7.7	11.1	21.4
Phosphate[d]	63.2	51.4	59.6	55.3	62.1	51.9	68.0	53.8	63.3	60.4	56.1	44.8	38.4	35.6	0.8
Total	**106.7**	**185.5**	**84.0**	**80.8**	**84.6**	**72.2**	**77.9**	**86.5**	**87.1**	**87.0**	**78.1**	**72.4**	**61.8**	**48.8**	**64.5**
±	***5.8***	***67.3***	***4.6***	***4.9***	***0.9***	***1***	***1***	***0.1***	***1.2***	***2.4***	***1.4***	***2.4***	***2.4***	***1***	***6.8***
CK6															
Olivine	17.8	48.5	36.4	10.2	16.2	196.6	71.0	43.5	10.8	27.4	24.1	37.8	27.0	44.0	53.9
±	*3.2*	*13.3*	*10.8*	*2.5*	*1.5*	*11.1*	*6.0*	*7.1*	*2.0*	*2.0*	*6.8*	*7.1*	*5.2*	*7.0*	*11.7*
High-Ca pyroxene	10.5	17.5	14.2	12.3	21.0	23.0	22.4	24.0	26.2	27.8	31.6	27.4	24.3	24.3	28.8
±	*2.4*	*4.7*	*3.3*	*2.9*	*5.7*	*5.4*	*5.5*	*5.6*	*7.1*	*7.0*	*7.1*	*6.9*	*6.3*	*6.2*	*9.4*
Plagioclase	24.1	12.4	19.9	8.8	10.5	101.6	44.1	8.6	15.6	15.2	9.8	/	10.5	9.7	7.9
±	*11.5*	*7.5*	*15.7*	*7.2*	*5.6*	*40.7*	*17.4*	*3.4*	*6.2*	*6.0*	*3.9*	/	*4.2*	*3.8*	*5.3*
Magnetite	8.6	42.5	8.0	5.6	20.2	/	/	7.7	5.4	/	4.8	7.6	6.8	15.3	/
±	*1.5*	*26.5*	*1.1*	*3.3*	*6.4*	/	/	*0.6*	*0.5*	/	*0.9*	*3.2*	*0.4*	*0.9*	/
Sulfide	0.7	1.2	1.6	0.1	/	/	/	1.9	/	2.1	/	0.8	1.0	2.9	0.4
Phosphate[e]	5.1	4.0	4.4	4.2	4.8	6.0	5.5	4.5	5.6	5.4	5.3	4.8	4.5	4.1	0.1
Total	**66.7**	**126.1**	**84.5**	**41.2**	**72.7**	**327.0**	**142.9**	**90.3**	**63.6**	**77.9**	**75.6**	**78.4**	**74.1**	**100.2**	**91.1**
±	***12.3***	***31.0***	***19.4***	***8.8***	***10.3***	***42.5***	***19.2***	***9.7***	***9.6***	***9.4***	***10.6***	***10.4***	***9.2***	***10.2***	***15.9***

[a] Values taken from CK4 NWA 5798.
[b] Values taken from CK3 NWA 5956.
[c] Values taken from CK5 EET92002.
[d] Values taken from CK5 EET92002.
[e] Values taken from CK4 NWA 5798.

mainly borne by olivine, plagioclase and high-Ca pyroxene. In this sample, calculated totals are acceptable, although slightly low for Yb, Lu and Hf (Table 4).

In the CK6 sample, the main carriers of LREE are plagioclase, olivine and high-Ca pyroxene and those of HREE are mainly olivine and high-Ca pyroxene. A lesser amount of REE is borne by magnetite and phosphate. Olivine is the main Hf carrier, followed by high-Ca pyroxene and plagioclase. Totals are acceptable, except for Nd (less than 50%, Table 4).

Thus, the mass-balance calculations show that REE are distributed among both phosphate and silicate phases (and sometimes magnetite). The part of phosphate in the REE budget tends to decrease when metamorphism degree increases, with the exception of CK5 A-881277 (Fig. 7a–c). In this sample, phosphate dominates the REE budget. Hafnium is only distributed among silicate phases; the part of Hf borne by phosphate is always negligible (Fig. 7d).

4. DISCUSSION

In the present study, the effect of the evolution of mineralogy and modal abundances coupled with the evolution of REE and Hf distribution among different mineral phases during increasing metamorphism in CK chondrites was examined.

4.1. Mineralogy abundances and evolution during metamorphism

Matrices made of phyllosilicates and low-Ca pyroxene only exist in chondrites affected by low grades of metamorphism. Matrix modal abundances are 47.3% (CV3) and 63.8% (CK3) in unequilibrated samples and decrease to less than 10% in CK4 NWA 5798. The matrix completely disappears in higher grade of metamorphism (Fig. 3a). The obtained values agree well with previously published data for CV chondrites (e.g. 50–51.3% in $CV3_{oxB}$, McSween, 1977) and CK chondrites (e.g. 57.7–86.7%, Righter and Neff, 2007). Low-Ca pyroxene abundance also decreases from type 3 (25.4% and 15.4%) to type 6, where it is absent. It is still present in the CK4 sample (14.6%), low in CK5 A-881277 (2.4%) and totally absent in CK5 EET92002 (Fig. 3a). High-Ca pyroxene does not display a clear evolution during metamorphism. It is less abundant in CK5 samples (2.9% in A-881277 and 1.9% in EET92002). The high occurrence of high-Ca pyroxene observed in this study, more particularly in CK4 samples in which total pyroxene is equal to 20%, contrasts with the results of Kallemeyn et al. (1991) where low-Ca and high-Ca pyroxenes are described as minor to accessory phases. The fact that the mask images calculated with XMapTools from X-ray maps allow to distinguish between phases that appear similar on BSE pictures (such as two types of pyroxene or pyroxene and olivine) likely explains these differences, together with the fact that no CK3 specimen was available for the study in 1991. Olivine forms a minor phase in CK3 chondrite (5.2%, almost exclusively in chondrules) while it reaches 17% in CV3, where it is only observed in chondrules. In equilibrated chondrites, olivine represents 54.1% in CK4 sample and more than 70% in types 5 and 6. Plagioclase appears from type 4 and does not appear to change during metamorphism. It only remains as a minor phase (up to 10%).

Accessory phases do not change significantly with increasing degree of metamorphism (Fig. 3b). Ilmenite and spinel, which occur as exsolutions in magnetite were not quantified or analyzed, even by EPMA, due to their very small sizes ($\leqslant$1 μm). Phosphate is the least abundant of the accessory phases. It is not observed in CV3, and ranges from 0.1% in CK6 to 0.8% in CK5 A-881277.

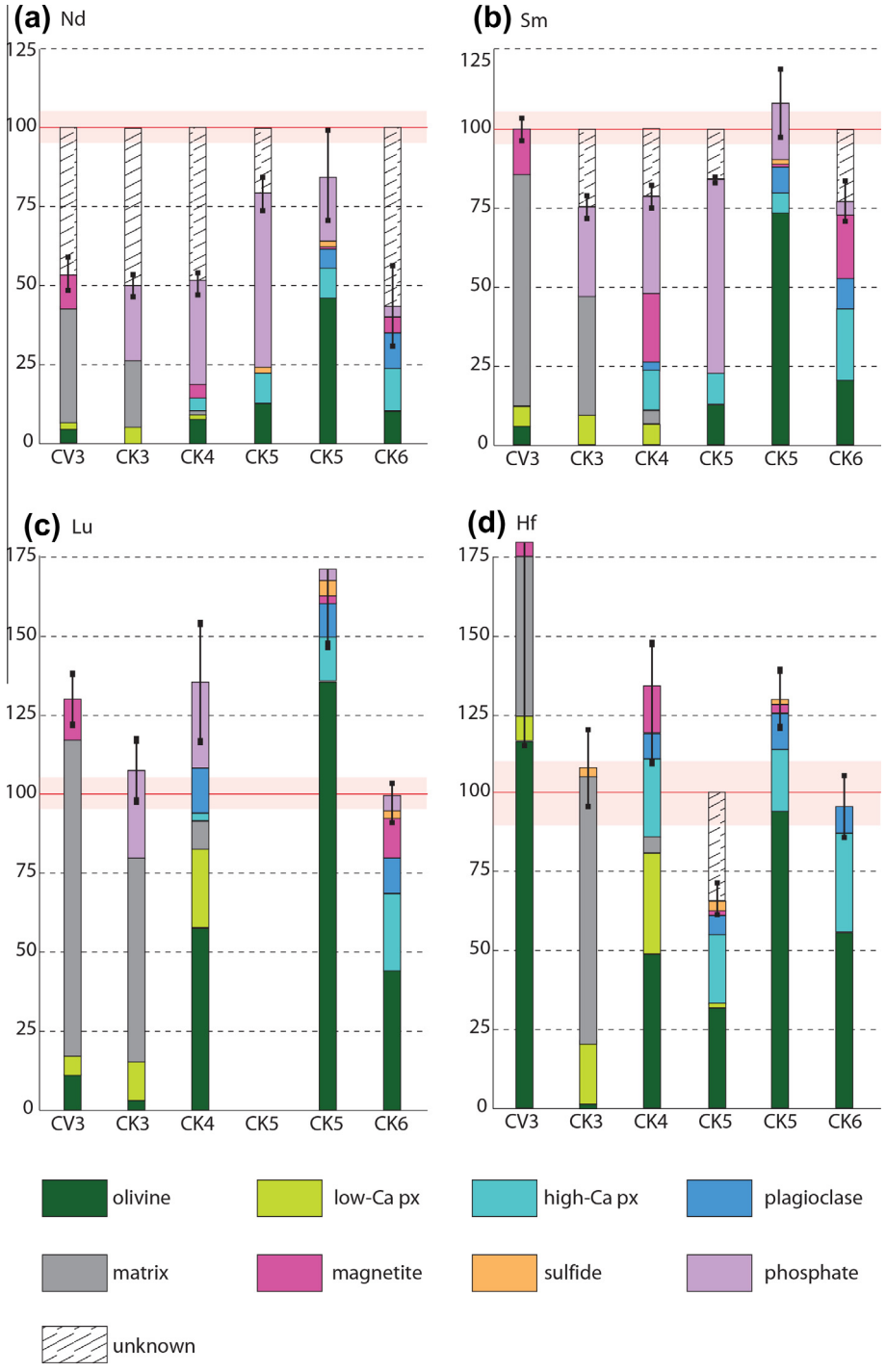

Fig. 7. (a) Nd, (b) Sm, (c) Lu and (d) Hf distribution among mineral phases in CV_{oxB} and CK chondrites.

Magnetite was not found in CK3, but a small amount of native Fe (0.2%), often altered into lawrencite, is observed. Magnetite represents only 1.6% in CV3 and ranges from 4.5% to 9.1% in metamorphozed CK samples. These values are compatible with those previous published (1.4–3.2% in $CV3_{oxB}$, McSween,1977 and 1.2–8.1%, in CK, Geiger and Bischoff, 1994), although the present values are slightly higher in CK chondrites (average = 6.9%, $n = 7$). Sulfide was not observed in the CV3 sample and it ranges from 2.6 in CK6 to 6.5% in CK5 A-881277. In all of the samples studied, except for CK6, in which also pyrrhotite is found, pentlandite is the only sulfide present.

The results of this study concur with those of Righter and Neff (2007), who described opaque assemblages in CK chondrites ranging from 3.5% to 18%, while Geiger and Bischoff (1994) described a maximum modal abundance of opaque phases of 1.3%, but usually lower than 0.1%. The difference between the results of Geiger and

Bischoff (1994) and this study might be related to the acquisition method. They used an image processing system coupled with a polarizing optical microscope whereas XMapTools involves EPMA X-ray maps based on chemical criteria. The latter, measured using WDS spectrometers, is expected to enable a more accurate and reliable determination of very small phases (minimal size 3–5 μm).

4.2. Origin of uncertainties in mass balance calculations

The samples are observed in detail with SEM to select areas for mapping as representative as possible of the whole rocks. Nevertheless, the mapped areas are only ± 1 mm^2 (Table 2), and may not be entirely representative for the whole rock. The samples on which two maps were performed (EET92002 and Y-82191) actually show some variations in modal abundances (Table 2) that can have an impact on mass balance calculations. In some cases (CK3, CK4 and CK5 EET92002), the mass balances appear better for HREE and Hf than for LREE. The missing LREE could be due to the higher incompatibility degree of these elements compared to that of the HREE. They are thus more sensitive to the 'nugget effect' of some micrometric or nanometric phases (e.g. phosphate, spinel, ilmenite...) that could explain the missing masses. The missing amount of some LREE could also be explained by weathering, but there is no clear correlation between the weathering stage indicated by Ba abundances (Table 3) and the total mass retrieved for LREE (Table 4). Calcium-Aluminum Inclusions (CAIs) are significantly enriched in REE and Hf (e.g. El Goresy et al., 2002; Huang et al., 2012) and relatively common in CV and CK chondrites. Even if any were observed in the studied polished sections or mapped areas, they could be present in the digested fractions and explain the missing LREE mass. Cerium could have distribution significantly different from that of other LREE, most likely due to its two oxidation states. The CV3 sample characterized here has an acceptable mass balance for almost all the REE (except Pr, Nd, Dy and Er), perhaps because it contains fewer mineral phases than the CK samples (respectively 5 and 7–9). Moreover, some measurements are missing due to the small size of crystals (e.g. high-Ca pyroxene in A-881277 and phosphate in all samples except NWA 5798 and EET92002), or only one measurement could be performed on the minerals (e.g. high-Ca pyroxene and phosphate in EET92002, and phosphates in NWA 5798). In that case, values for calculations are taken from other sample (see Table 3, footnotes). When only one measurement is available, we have no information about variability of contents, that can explain a part of the uncertainties in the mass balances.

4.3. Are phosphates the key to explain Lu–Hf whole-rock discrepancies?

This study shows that silicates and magnetite can contribute significant proportions of whole-rock REE in CK and CV chondrites. In most cases, whole-rock REE budgets are not dominated by phosphates only. Phosphates are considered to dominate the REE budget in ordinary chondrites (Brearley and Jones, 1998). Thus, it is assumed that their recrystallization during metamorphism can lead to Lu/Hf heterogeneities (Bouvier et al., 2008). In the present study, we investigated the REE and Hf distribution among minerals in the only highly metamorphosed suite of carbonaceous chondrites. The amount of phosphate in CK chondrites is low (0.1–1%), with no clear evolution of abundance during metamorphism (the highest abundance is found in CK5 and the lowest in CK6). Two phosphate species are observed: apatite or Cl-apatite in CK3 and merrillite in all the other samples. They either represent mineralogical evolution of phosphate during metamorphism or the natural variability in chondritic samples. The REE and Hf concentrations obtained in CK phosphates in this study and the values already published for Sm and Nd (Amelin and Rotenberg, 2004) and Lu and Hf (Amelin, 2005) on OC (H5, L/LL4, L4, L5) are compared. The values obtained for REE on CK phosphate are in general agreement with those previously published, although they are lower for LREE in CK5 EET92002 (Fig. 6c). Hafnium contents in CK chondrites appear at least 2 times higher than in OC (Fig. 6c).

This study shows that silicates could host significant parts of REE, together with phosphates in CK and CV chondrites, except in sample A-881277. In this sample, the contribution of phosphate to the REE mass balance is 40–70%. This sample displays peculiar features such as a high enrichment in HREE ($(La/Yb)_N = 2.2$) and sulfide with elevated Co concentrations (12,500 ppm), whereas the latter ranges from 200 to 1000 ppm in other samples. We thus assume that CK5 A-881277 experienced different conditions than the other CK meteorites presented in this paper and the contribution of phosphate to REE mass balance likely represents a maximum value. In the other samples, phosphate still constitutes an important contributor for REE. LREE (Sm and Nd) and HREE (Lu) have not the same distribution among mineral phases. Phosphates bear up to 25–50% of LREE in types 3–5, and the remaining is distributed in silicates (mainly matrix for type 3 and olivine and high-Ca pyroxene in types 4 and 5) (Fig. 7a and b). In the CK6 sample, Sm and Nd appear only borne by silicates and magnetite (less than 7% in phosphate). Nevertheless, CK6 sample has the lowest phosphates abundance (0.1%) and the apparent decreasing of phosphate part in the LREE mass balance could be an artifact due to the selection of non-representative areas for mapping. Thus, the Sm and Nd fractions stored in phosphate likely escape redistribution at least since metamorphism grade remains moderate (below type 6), while the fraction of Sm and Nd borne by silicates is redistributed during metamorphism. In CK3 and CK4 samples, $\sim 30\%$ of Lu is actually borne by phosphate, but matrix in CK3 as well as olivine and both low- and high-Ca pyroxene in CK4 account for more than 50% of the Lu fraction (Fig. 7c). In higher metamorphic grades, the fraction of Lu borne by phosphate drops below 10%. The remaining fraction is distributed among silicates (CK5) and silicates and magnetite (CK6). Similar to the LREE, a significant, even major, part of Lu is redistributed during highest grades of metamorphism. On the contrary to that observed for Sm and Nd, the decrease of the Lu fraction borne by phosphate between type 4 and type 5 might not due to the decline of merrillite modal

abundance (0.4% in CK4 and 0.6% in CK5, Fig. 7c). It could rather be due to diminishing Lu concentrations in phosphate (one order of magnitude lower in CK5 than in CK4, Table 2) but since only one measurement was performed in each crystal, this result should be taken carefully. In CV3 NWA 5772, in which no phosphate was observed, the matrix – composed of a mixture of minerals with affinities to cronstedite, chrysotile and saponite – is the main carrier, together with magnetite for LREE. The fraction of Hf borne by phosphate is always negligible (less than 0.8%, Fig. 7d). Whatever the chondrite type and class, Hf is essentially concentrated in matrix (CK3) and in olivine, and low- and high-Ca pyroxenes. Considering that metamorphism induces low-Ca pyroxene and matrix breakdown in parallel with an olivine modal abundance increase, Hf is significantly re-distributed during metamorphism.

Up to 30% of Sm and Nd are stored in phosphates in CK chondrites of types 3–5, and are not significantly redistributed during metamorphism. This behavior may explain the robustness of the Sm/Nd ratios in chondrites through metamorphism, and the slight discrepancies observed in the present-day isotopic Nd values. On the contrary, Lu and more particularly Hf are mostly borne by several different minerals and consequently they are redistributed during metamorphism–induced recrystallization. The Lu/Hf ratios are therefore significantly disturbed during chondrites metamorphism, and the evolution of these rocks with different Lu/Hf during 4.5 Ga lead to the big discrepancies in Hf present-day values.

5. CONCLUSIONS

To conclude, this study of REE and Hf distribution among mineral phases in a set of five CK and one CV3 chondrites highlights that:

- REE are hosted in both phosphate and silicates. Up to 40% of Sm and Nd and 30% of Lu are stored in phosphates in low grade of metamorphism, the remaining being in silicates.
- Phosphate in one peculiar CK5 sample hosts up to 65% of LREE and 35% of HREE, that could represents a maximum value.
- Hf is only distributed among silicates. The phosphate does not participate to the Hf mass balance.
- Sm and Nd are (re)distributed among the same mineral phases during metamorphism. This coupling preserves the Sm/Nd ratio, and consequently the uniformity of Nd chondritic values.
- Lu and Hf are not borne by the same minerals. Lu is redistributed from phosphate to silicate phases with increasing degree of metamorphism, while Hf is stored in olivine and high-Ca pyroxene in types 4–6. This decoupling can create major discrepancies in the Lu/Hf ratio, and can thus explain the heterogeneity observed in present-day $^{176}Hf/^{177}Hf$ values.

These results are obtained on CV and CK carbonaceous chondrites and may be different in other classes of chondrites. However, the dichotomy highlighted in Sm, Nd and Lu, Hf behavior during metamorphism could likely be observed in all chondrite classes. Thus, it could be better to focus on chondrites with low grades of metamorphism to determine CHUR parameters for Lu–Hf system, as already suggested by Bouvier et al. (2008).

ACKNOWLEDGMENTS

The authors acknowledge Oscar Steenhaut (VUB) and Alain Bernard (ULB) for SEM analyses, Michel Fialin and Frédéric Couffignal for EPMA, and Andrei Izmer for assistance with LA-ICP-MS analyses. The authors are grateful to Jeff Vervoort, Timothy Fagan and an anonymous reviewer for their help and useful comments. C.M. is grateful to Fabien Kuntz for having given pieces of NWA 5772 sample. This work benefited from funding from the Belgian Science Policy Office (SAMBA and BELAM programs) and the InBev-Baillet Latour Antarctica Fellowship. Ph. C and F. V. thank Research Foundation Flanders (FWO) for grant G.A078.11 and G.0021.11. S.G. is a postdoctoral fellow of the Research Foundation - Flanders (FWO). V.D. thanks the FRS-FNRS for present funding.

REFERENCES

Amelin Y. (2005) Meteorite phosphates show constant 176Lu decay rate since 4557 million years ago. *Science* **310**, 839–841.

Amelin Y. and Rotenberg E. (2004) Sm–Nd systematics of chondrites. *Earth Planet. Sci. Lett.* **223**, 267–282.

Anthony J.W, Bideaux R.A, Bladh K.W, and Nichols M.C, Eds., Handbook of Mineralogy, Mineralogical Society of America, Chantilly, VA 20151-1110, USA. http://www.handbookofmineralogy.org/.

Barrat J. A., Zanda B., Moynier F., Bollinger C., Liorzou C. and Bayon G. (2012) Geochemistry of CI chondrites: Major and trace elements, and Cu and Zn isotopes. *Geochim. Cosmochim. Acta* **83**, 79–92.

Blichert-Toft J. and Albarède F. (1997) The Lu–Hf isotope geochemistry of chondrites and the evolution of the mantle-crust system. *Earth Planet. Sci. Lett.* **148**, 243–258.

Bouvier A., Vervoort J. D. and Patchett P. J. (2008) The Lu–Hf and Sm–Nd isotopic composition of CHUR: Constraints from unequilibrated chondrites and implications for the bulk composition of terrestrial planets. *Earth Planet. Sci. Lett.* **273**, 48–57.

Brearley A. J. (1997) Disordered biopyriboles, amphibole, and talc in the Allende meteorite: Products of nebular or parent body aqueous alteration? *Science* **276**, 1103–1105.

Brearley A. J. and Jones R. H. (1998) Chondritic meteorites. *Rev. Mineral.* **36**, XV–XVI.

De Andrade V., Vidal O., Lewin E., O'Brien P. and Agard P. (2006) Quantification of electron microprobe compositional maps of rock thin sections: An optimized method and examples. *J. Metamorph. Geol.* **24**, 655–668.

El Goresy A., Zinner E., Matsunami S., Palme H., Spettel B., Lin Y. and Nazarov M. (2002) Efremovka 101.1: A CAI with ultrarefractory REE patterns and enormous enrichments of Sc, Zr, and Y in Fassaite and Perovskite. *Geochim. Cosmochim. Acta* **66**, 1459–1491.

Gannoun A., Boyet M., El Goresy A. and Devouard B. (2011) REE and actinide microdistribution in Sahara 97072 and ALHA77295 EH3 chondrites: A combined cosmochemical and petrologic investigation. *Geochim. Cosmochim. Acta* **75**, 3269–3289.

Geiger T. and Bischoff A. (1994) Formation of opaque minerals in CK chondrites. *Planet. Space Sci.* **43**, 485–498.

Hollocher K., Fakhry A. and Ruiz J. (1995) Trace element determination for USGS basalt BHVO-1 and NIST standard reference materials 278, 688 and 694 by inductively coupled plasma-mass spectrometry. *Geostandard. Newslett.* **19**, 35–40.

Huang S., Farkaš J., Yu G., Petaev M. I. and Jacobsen S. B. (2012) Calcium isotopic ratios and rare earth element abundances in refractory inclusions from the Allende CV3 chondrite. *Geochim. Cosmochim. Acta* **77**, 252–265.

Jacobsen S. B. and Wasserburg G. J. (1979) The mean age of mantle and crustal reservoirs. *J. Geophys. Res.* **84**, 7411–7427.

Jacquet E., Gounelle M. and Alard O. (2012) Trace-element microdistribution in carbonaceous chondrite chondrules. *Lunar Planet. Sci. Conf*. The Woodlands, Texas.

Jochum K. P. and Stoll B. (2008) Reference materials for elemental and isotopic analyses by LA-(MC)-ICP-MS: Successes and outstanding needs, Laser Ablation ICP-MS in the Earth Sciences: Current practices and outstanding issues. *Mineral. Assoc. Can.* **40**, 147–168.

Kallemeyn G. W., Rubin A. E. and Wasson J. T. (1991) The compositional classification of chondrites: V. The Karoonda (CK) group of carbonaceous chondrites. *Geochim. Cosmochim. Acta* **55**, 881–892.

Kong P., Deloule E. and Palme H. (2000) REE-bearing sulfide in Bishunpur (LL3.1), a highly unequilibrated ordinary chondrite. *Earth Planet. Sci. Lett.* **177**, 1–7.

Lanari P., Guillot S. p., Schwartz S. p., Vidal O., Tricart P., Riel N. and Beyssac O. (2012) Diachronous evolution of the alpine continental subduction wedge: Evidence from P, T estimates in the Briançonnais Zone houillère (France, Western Alps). *J. Geodyn.* **56–57**, 39–54.

Lanari P. (2013) Deciphering high-pressure metamorphism in collisional context using microprobe mapping methods: Application to the Stak eclogitic massif (northwest Himalaya). *Geology* **41**(2), 111–114.

Mason B. and Martin P. M. (1974) Minor and trace element distribution in melilite and pyroxene from the Allende meteorite. *Earth Planet. Sci. Lett.* **22**, 141–144.

McSween Jr H. (1977) Petrographic variations among carbonaceous chondrites of the Vigarano type.. *Geochim.Cosmochim.i.Acta* **41**(12), 1777–1790.

Patchett P. J., Vervoort J. D., Söderlund U. and Salters V. J. M. (2004) Lu, Hf and Sm, Nd isotopic systematics in chondrites and their constraints on the Lu, Hf properties of the Earth. *Earth Planet. Sci. Lett.* **222**, 29–41.

Righter K. and Neff K. E. (2007) Temperature and oxygen fugacity constraints on CK and R chondrites and implications for water and oxidation in the early solar system. *Polar Sci.* **1**, 25–44.

Weisberg M. K., McCoy T. J. and Krot A. N. (2006) Systematics and evaluation of meteorite classification. In *Meteorites and the Early Solar System II* (eds. D. S. Lauretta and , Jr.H. Y. McSween). The University of Arizona Press.

Weisberg M. K., Prinz M., Clayton R. N. and Mayeda T. K. (1997) CV3 chondrites; three subgroups, not two. *Meteorit. Planet. Sci.* **32**, 138–139.

Yongheng C., Daode W. and Pernicka E. (1993) REE and other trace element chemistry of oldhamite (CaS) in the Qingzhen chondrite (EH3) and their genetic implications. *Chin. J. Geochem.* **12**, 317–327.

Associate editor: Maud Boyet